Thermalhydraulics of Flowing Particle-Bed-Type Fusion Reactor Blankets

R.E. Nietert, S.I. Abdel-Khalik
Nuclear Engineering Department,
University of Wisconsin, 1500 Johnson Drive, Madison, Wisconsin 53706, U.S.A.

Abstract

An experimental investigation has been conducted to determine the heat transfer characteristics of gravity-flowing particle beds. A heat transfer loop has been constructed for such a purpose. Glass microspheres have been allowed to flow by gravity at controlled rates through an electrically heated stainless steel tubular test section. Values of the local and average convective heat transfer coefficient as a function of the average bed velocity, particle size and heat flux have been determined. Such information is necessary for the design of gravity flowing particle-bed type fusion reactor-blankets and associated tritium recovery systems.

I. Introduction

An experimental investigation has been conducted to examine the heat transfer characteristics of gravity-flowing particle bed type fusion reactor blankets. In one such design, proposed by the University of Wisconsin fusion reactor study group for the laser fusion reactor SOLASE (1,2), lithium oxide particles 100-200 μm in diameter, flow under the influence of gravity through the blanket and serve both as a tritium breeder and heat transport medium. The entire modular, spherical blanket is made from graphite with honeycomb type construction. The particle velocity distribution is tailored to match the neutron heat deposition as it decreases radially away from the first wall.

These blanket designs offer many advantages including low cost, low weight, low induced radioactivity levels, the potential for hands on maintenance, modular construction, low pressure, adequate breeding, low tritium inventory and leakage, and sufficiently long life. Another significant advantage is the ability to decouple the first wall and blanket coolant/breeder temperatures where the first wall is operated at a significantly different temperature than that of the coolant. This is possible because of the expected low heat transfer coefficient between the flowing particle stream and the first wall. The temperature of the flowing particle bed, where most of the fusion neutron energy is directly deposited, is dictated by power cycle efficiency requirements. The first wall temperature, on the other hand, can be selected on the basis of radiation damage considerations.

Analyses of the performance of these blankets and associated power cycle and tritium recovery equipment have been hampered by lack of data for the convective heat transfer coefficients in flowing particle beds and their dependence on the different design and operational parameters, viz. average channel velocity, blanket module geometry and size, particle size, and particle size distribution. To this end, this investigation has been undertaken. Such data are necessary in order to obtain realistic estimates of the temperature distribution within the blanket structure. This information, in turn, is needed in estimating the stress levels within the blanket structure. Accurate estimates of the convective heat transfer coefficients are critically needed for the design of the tritium recovery system inasmuch as the diffusion coefficient is a strong function of temperature.

The aim of this investigation is to experimentally determine the heat transfer coefficient for flowing particle beds and how it is affected by the average bed velocity and particle size. A heat transfer loop has been constructed for such a purpose. The experimental equipment and procedure are described in Section II while the results are given in Section III. Conclusions and recommendations are given in Section IV.

II. Experimental Equipment and Procedure

II.1. Experimental Equipment

Figure 1 is a schematic diagram of the heat transfer loop. Solid soda-lime glass particles of controlled size distribution flow by gravity from the upper storage tank through an entrance region 29 cm in length before entering the test section. The test section is an electrically heated Type 321 stainless steel tube, 54 cm long with a 1.43 cm outside diameter and 0.025 cm wall thickness. From the test section, the particles flow through a 36 cm exit region into the lower collection tank. The particle flow rate through the test section is controlled by means of a sliding cone valve assembly located at the lower

end of the tube exit region. A scale is used to measure the mass flow by weighing the particles collected in a metal bucket over a measured period of time. The particles are then cooled and returned to the upper storage tank via a counter flow shell and tube heat exchanger. This return is accomplished by a large suction pump located on the top of the upper storage tank and is aided by injection of high-pressure air into the shell side of the heat exchanger. The particle return heat exchanger and the upper storage tank inlet are lined with high strength glass to minimize erosion of the loop by the particles.

A photograph of the test section is shown in Figure 2. Electric current from a 50 kW DC power supply is passed through the tube walls. The power input is controlled by placing a resistor bank in series with the tube resistance. The test section is thermally insulated from the outside by a cylindrical composite wall consisting of an outer layer of fiber glass and an inner layer of high temperature organic impregnated fibrous glass. The test section is electrically insulated from the entrance and exit regions and support frame by mounting the ends of the tube in ceramic sleeves placed on horizontal asbestos-concrete boards. The sleeves allow the test section to expand freely in the vertical direction when it is heated.

The wall temperature distribution along the flow direction is measured by means of Chromel-Alumel thermocouples spot welded onto the outer tube surface (Fig. 2). A thermocouple is also used to measure the particle inlet bulk temperature; these temperatures are recorded on a twenty channel continuously scanning Type K Honeywell chart recorder.

The power input to the test sections is determined by measuring the voltage drop across the tube and the current through a shunt in series with the tube resistance. Standard volt meters are used in this regard. The wall temperature distribution, power input, and particle inlet temperature are used to determine the local and average heat transfer coefficients along the test section.

The radial temperature distribution of the particles at the test section exit is also measured by means of a Chromel-Alumel thermocouple probe mounted on a micrometer assembly placed upstream of the flow control valve. The thermocouple output is measured using a Fluke digital thermometer. The heat transfer loop with the test section exposed is shown in Figure 3.

II.2. Experimental Procedure

The experiment is operated in a steady state mode by continuously circulating the particles through the loop. The experiment is conducted for different power levels, particle sizes, and flow rates.

Initially, the complete inventory of glass particles is placed in the lower collection tank. The heat exchanger cooling water and air injection are first turned on. With the control valve closed, the glass particles are then pumped to the upper storage tank. Once the lower collection tank has been emptied, the suction pump is momentarily shut off to allow the tube above the control valve to become packed with particles. The suction pump is once again started and the control valve is adjusted to its fully-open position. The particles are allowed to flow around the loop without heating for approximately thirty minutes to establish steady state flow conditions. The resistor bank connected in series with the test-section is adjusted to obtain the desired power input to the tube (600, 800 or 1000 W). The power supply is turned on. The particle radial exit temperature profile probe is placed at the tube wall and the axial wall temperatures are monitored until steady

state conditions are reached. At that time, all wall temperature readings, power input, and particles' inlet temperature are recorded. The exit temperature profile is then measured by moving the micrometer-mounted probe at approximately 0.06 cm radial intervals. The flow rate is measured by collecting the particles exiting the control valve into a metal container for a measured period of time.

At this point, preparations are made to conduct the experiment at the next lower flow rate. The control valve is constricted in a pre-calibrated fashion to obtain the required mass flow. Again, the temperatures are monitored until the new steady state conditions are reached. This requires a waiting period of about thirty to forty minutes. Experiments at lower mass flow rates follow. A total of nine flow rates are examined at each power level.

The resistor bank is adjusted and data for all nine flow rates are again collected for two additional power levels. The loop is thoroughly cleaned and all three power levels are repeated for the second particle size studied. Thus a total of fifty four experiments have been conducted. Table 1 lists the ranges of experimental variables examined in these experiments. Experiments using two other tube sizes, a third particle size, and an alternate particle material are planned.

III. Experimental Results

III. 1. Data Reduction

The test section has been divided along the flow direction using a twenty six node finite difference scheme. This nodal spacing has been used to analyze all the collected data. A 64 K microcomputer manufactured by Smoke Signal Co. has been used to process the data. Such factors as: 1) variation of specific heat capacity with particles' exit temperature (3), 2) variation of nodal tube length with local wall temperature, cross sectional area, and surface area variations with temperature, 3) variation of nodal tube resistance with temperature and its impact on the local heat flux values, and 4) radiation losses from the tube wall to the particles have been accounted for.

An energy balance over the test section using the known power input, particle flow rate, and inlet temperature has been used to calculate the particle bulk exit temperature. An iterative scheme is required to account for the dependence of particles' specific heat on temperature.

Calculation of all nodal wall linear dimensions has been made using equation (1)

$$L_i = L_{io}\left[1 + \beta\,(T_{wi} - T_o)\right]. \qquad (1)$$

Here, T_{wi} is the outer surface wall temperature of node i, T_o is a reference temperature at which the nodal wall linear dimension, L_{io}, has been measured, and β is the temperature coefficient of expansion. The value of β for type 321 stainless steel is $12 \times 10^{-6} {}^{\circ}K^{-1}$ (4).

The resistivity, ρ_i, of node i has been computed using the relation:

$$\rho_i = \rho_o\left[1 + C\,(T_{wi} - T_o)\right] \qquad (2)$$

where ρ_o is the resistivity at the reference temperature T_o, and C is the temperature coefficient of resistivity. The value of C for type 321 stainless steel is $0.00169 {}^{\circ}K^{-1}$ (5). Values of the different node resistances have then been calculated using the corrected values of resistivity, length, and cross sectional area. The above corrections are necessary because of the large temperature variations along the tube.

A finite difference scheme with thirteen axial nodes has been used to determine the bulk

temperature distribution of the particle bed along the flow direction using a simple steady state energy balance. Linear interpolation is used to determine the particles' bulk temperature at other locations.

A gray body formulation has been used to compute the local radiative heat flux. The configuration factor between any given tube wall node and the adjacent particle node is taken to be unity so that

$$q''_{ri} = \varepsilon\sigma \left(T_{wi}^{\,4} - T_{pi}^{\,4}\right) \tag{3}$$

where q_{ri} is the radiative heat flux, T_{wi} is the nodal wall temperature, T_{pi} is the local particle bulk temperature, ε is the wall emissivity, and σ is the Stefan-Boltzman constant. A value of $\varepsilon = 0.3$ has been used (6). The above formulation assumes the particle bed to behave as a black body.

The local convective heat flux and heat transfer coefficient for each node are next calculated using equations (4) and (5)

$$q''_{ci} = \frac{QR_i}{R_{tot}} \frac{1}{\pi D_i L_i} - q''_{ri} \tag{4}$$

$$h_{loc,i} = \frac{q''_{ci}}{T_{wi} - T_{pi}} \tag{5}$$

where Q is the power input to the tube, R_i is the resistance of node i, R_{tot} is the total resistance of the tube, D_i is the inside diameter of the tube for node i, and L_i is its length.

The average convective heat flux along the tube is calculated using the local convective heat flux values as shown in equation (6). This is then used to determine the overall average heat transfer coefficient based on the logarithmic mean temperature difference between wall and particle nodal temperatures at inlet and exit as shown in equation (7)

$$q''_{c,tot} = \sum_i \frac{q''_{ci}\, \pi D_i L_i}{A_{tot}} \tag{6}$$

$$\bar{h}_c = \frac{q''_{c,tot}}{\Delta T_{ln}} \tag{7}$$

where A_{tot} is the total wall surface area, ΔT_{ln} is the logarithmic mean temperature difference, $q''_{c,tot}$ is the average convective heat flux, and h_c is the overall average convective heat transfer coefficient.

III. 2. Results

Typical results showing the wall temperature distribution along the tube wall as a function of axial distance from heated tube inlet and average bed velocity are given in Figure 4. These are the outside surface temperatures measured by the Chromel-Alumel thermocouples welded onto the tube wall. The wall temperature is shown to increase rapidly at first followed by a nearly linear increase away from the tube inlet. The wall temperature is significantly reduced as the average bed velocity increases. Results similar to those in Fig. 4 for other power inputs, particle size, and average bed velocity have been obtained.

Dependence of the wall temperature distribution on particle size for the same power input and mass flow rate is shown in Fig. 5. These results indicate that smaller particles tend to "wet" the tube surface more effectively than the larger particles resulting in a larger heat transfer coefficient and, thus, a somewhat lower wall temperature along the entire length of the heated tube.

Typical results showing the radial temperature distribution for the particles at the tube exit for different values of average bed velocity are given in Figure 6. The particles' temperatures are plotted as a function of the nondimensional radial distance away from the tube center line. These profiles correspond to an axial elevation approximately 37 cm downstream from the heated section. These profiles are expected to be somewhat flatter than those at the heated test section exit because of radial heat conduction. The differences however are expected to be small especially in the central region because of the low particle conductivity. Fig. 6 shows that the particle temperature decreases rapidly with increasing bed velocity. The radial profile closely approximates that of plug flow as the average velocity is increased. However, for low velocity, the plug flow approximation is clearly inadequate.

Figure 7 shows the effect of particle size on the radial temperature profile. Larger size particles result in a "flatter" temperature distribution.

Typical results showing the local convective heat transfer coefficient along the tube wall as a function of axial distance from tube inlet and average bed velocity are shown in Figure 8. The local heat transfer coefficient is shown to decrease with axial distance and is quite sensitive to the particle average velocity. These coefficients are quite low varying between 0.03 and 0.08 $W/cm^2°K$ and increase with average bed velocity.

In Figure 9, values of the local heat transfer coefficient along the tube wall are compared for different power levels (heat fluxes). Although a change in scale has been made, a definite dependence on the heat flux is demonstrated. The heat transfer coefficient consistently increases with increasing heat flux along the axial length of the heated tube. This indicates a strong dependence of the heat transfer coefficient on the physical properties of the particles.

Figure 10 shows the effect of particle size on the local heat transfer coefficient versus average bed velocity for the smaller size particles used in this study. The average heat transfer coefficient is shown to increase with average bed velocity for a given heat flux and with heat flux for a given average velocity. These heat transfer coefficients, however, are quite low being only between 0.02 and 0.05 $W/cm^2°K$.

Figure 12 shows the effect of particle size on the average heat transfer coefficient. The average heat transfer coefficient increases with decreasing particle size. From Figures 11 and 12 the average heat transfer coefficient is found to vary with average particle velocity to approximately the 0.4 power.

IV. Conclusions and Recommendations

A heat transfer loop has been constructed and used to determine the local and average heat transfer coefficients of gravity flowing particle beds as functions of the average bed velocity, heat flux, and particle size. The overall average heat transfer coefficient is found to vary with average bed velocity to approximately the 0.4 power and its magnitude is quite low being nearly 0.04 $W/cm^2°K$ at an average bed velocity of 10 cm/sec and heat flux of 3.43 W/cm^2. Such low values confirm the feasibility of the temperature decoupling concept (7) where the first wall is operated at a temperature significantly different from that of the blanket coolant. The former can therefore be selected on the basis of radiation damage considerations while the latter is dictated by power cycle efficiency requirements.

Additional experiments over a wider range of variables are planned. Among these varia-

bles are particle sizes, particle size distribution, particle physical properties, average bed velocity, and channel geometry. The heat transfer loop used in this study has been modified and this work is currently underway. The ultimate goal is to obtain generalized Nusselt-type correlations for the heat transfer coefficients in gravity flowing particle beds.

References

[1] CONN, R.W. et al., "SOLASE-A Laser Fusion Reactor Study," University of Wisconsin Report, UWFDM-220 (December 1977).

[2] ABDEL-KHALIK, S.I. et al., "A Novel Blanket Design for ICTRs," Proc. Third Topical Meeting on the Technology of Controlled Nuclear Fusion, Santa Fe, NM (May 1978).

[3] TOULOUKIAN, Y.S., BUYCO, E.H. (Eds.), Thermophysical Properties of Matter, IFI/Plenum (1970).

[4] SHORTLEY, G., WILLIAMS, D., Elements of Physics, Prentice Hall, (1971).

[5] KNOWLTON, A.E. (Ed.) et al., Standard Handbook for Electrical Engineers, McGraw Hill, (1941).

[6] SIEGEL, R., HOWELL, J.R., Thermal Radiation Heat Transfer, McGraw Hill, (1972).

[7] ABDEL-KHALIK, S.I., CONN, R.W., MOSES, G.A., "Engineering Problems of Laser-Driven Fusion Reactors," Nuclear Technology, 43, 5-21, (1979).

Nomenclature

A_{tot}	total wall surface area, corrected for temperature expansion
C	temperature coefficient of resistivity
D_i	nodal inside diameter, corrected for temperature expansion
$\bar{h}_c$	overall average convective heat transfer coefficient
$h_{loc,i}$	local convective heat transfer coefficient at node i
L_i	nodal length, corrected for temperature expansion
L_{io}	nodal length at reference temperature T_o
Q	total power input
q''_{ci}	local convective heat flux at node i
$q''_{c,tot}$	average convective heat flux along the entire tube
q''_{ri}	local radiative heat flux at node i
R_i	nodal resistance, corrected for temperature
R_{tot}	total tube resistance
T_o	reference temperature
T_{pi}	particle bulk temperature for node i
T_{wi}	nodal wall temperature
ΔT_{ln}	logarithmic mean temperature difference between wall and particles at inlet and exit
β	temperature coefficient of expansion
ε	tube wall emissivity
ρ_i	nodal resistivity, corrected for temperature
ρ_o	tube wall resistivity at reference temperature T_o
σ	Stefan-Boltzman constant

Table 1

Ranges of Experimental Variables

Tube inside diameter (cm)	1.38
Particle Size (μm)	(177-250), (420-590)
Power input (W)	600-1000
Average bed velocity (cm/sec)	3.5-15.0

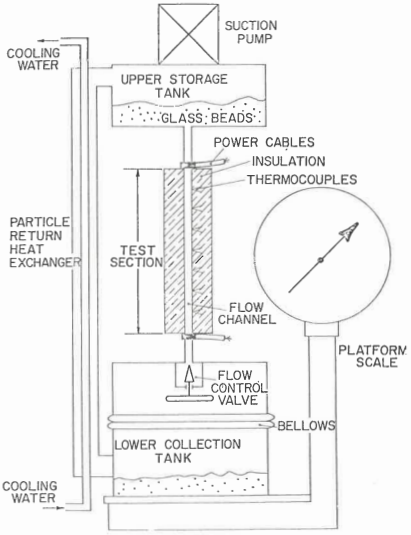

Fig. 1 Schematic diagram of the test loop used in this study.

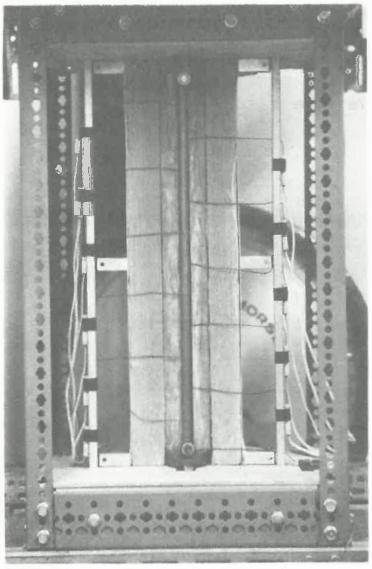

Fig. 2 Photograph of the heated test section showing the surface thermocouples and outer insulation.

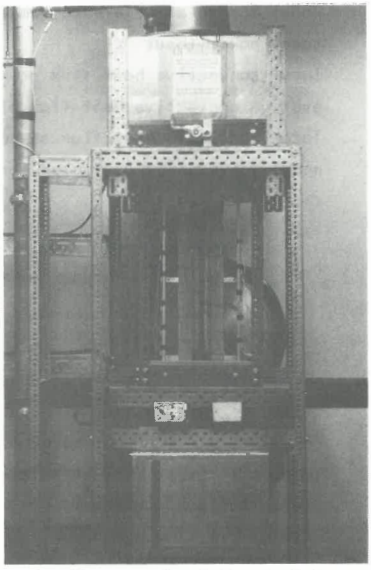

Fig. 3 Photograph of the test loop with exposed test section.

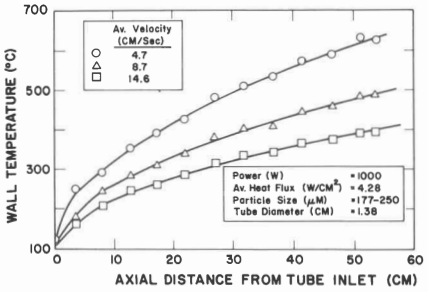

Fig. 4 Variation of wall temperature along the tube surface for different bed velocities.

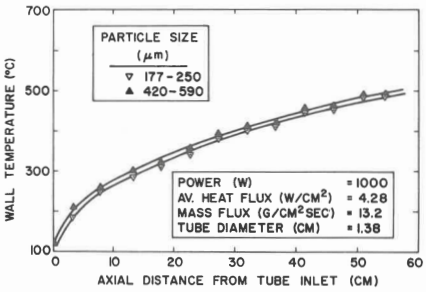

Fig. 5 Results showing dependence of wall temperature distribution on particle size.

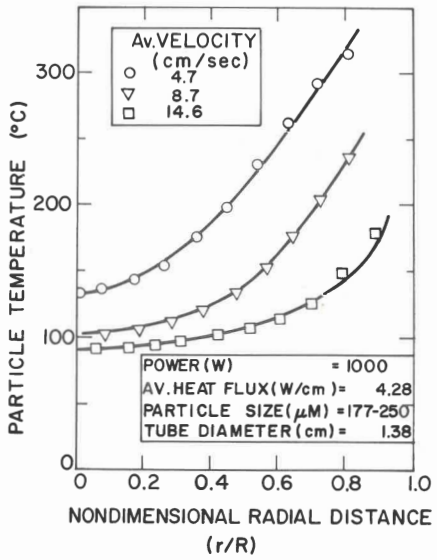

Fig. 6 Radial particle temperature distribution at tube exit for different bed velocities.

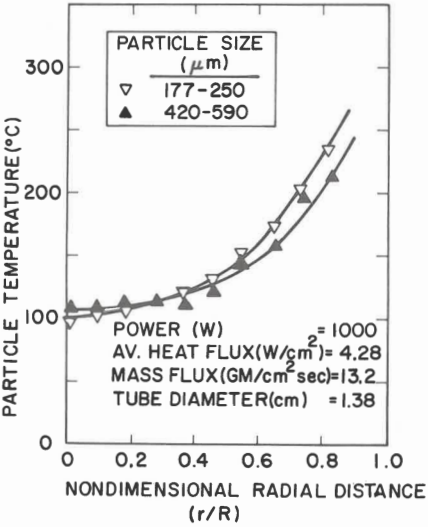

Fig. 7 Results showing dependence of radial particle temperature distribution on particle size.

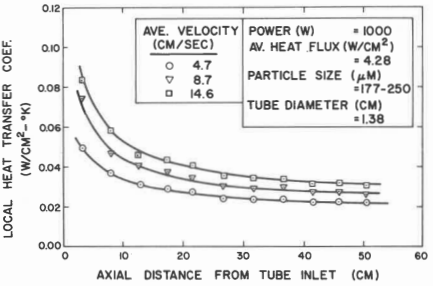

Fig. 8 Variation of the local heat transfer coefficient along the tube for different bed velocities.

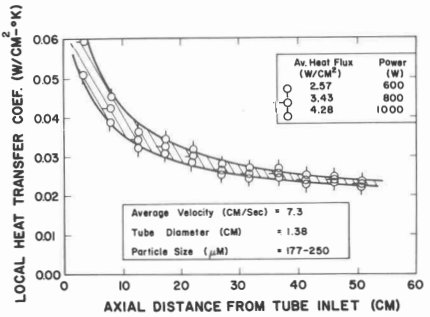

Fig. 9 Results showing dependence of local heat transfer coefficients on power level.

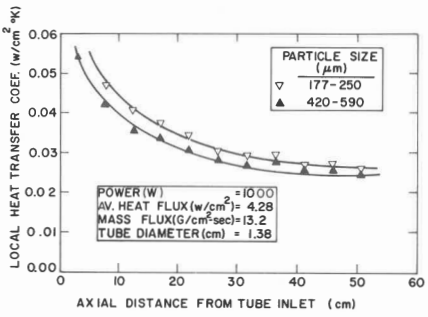

Fig. 10 Results showing dependence of local heat transfer coefficients along the tube on particle size.

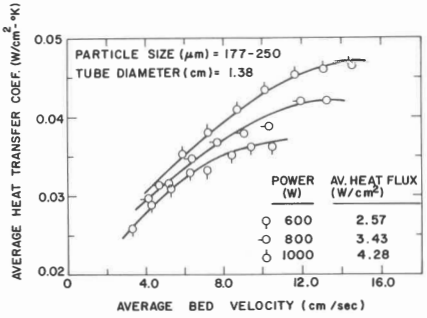

Fig. 11 Average heat transfer coefficients as functions of bed velocity and average heat flux.

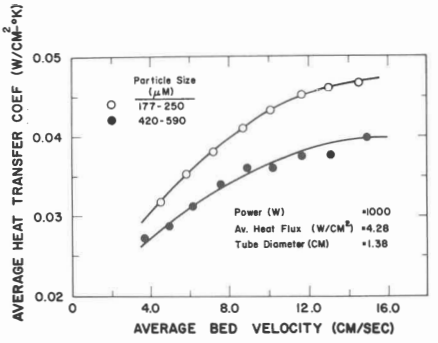

Fig. 12 Results showing the effects of particle size on the average heat transfer coefficient.